PHILOSOPHICAL TRANSACTIONS OF THE ROYAL SOCIETY A MATHEMATICAL, PHYSICAL & ENGINEERING SCIENCES

# New Ways of Characterizing Layered Silicates and their Intercalates

J. M. Thomas

*Phil. Trans. R. Soc. Lond. A* 1984 **311**, 271-285
doi: 10.1098/rsta.1984.0028

*Phil. Trans. R. Soc. Lond.* A **311**, 271–285 (1984) [ 271 ]
*Printed in Great Britain*

# New ways of characterizing layered silicates and their intercalates

By J. M. Thomas, F.R.S.
*Department of Physical Chemistry, University of Cambridge, Lensfield Road, Cambridge CB2 1EP, U.K.*

[Plates 1–3]

Four new methods of probing the atomic and microstructural characteristics of the clay minerals are described: solid-state, magic-angle-spinning $^{27}Al$ and $^{29}Si$ n.m.r. (along with $^{13}C$ n.m.r. of mobile, intercalated organic species); X-ray induced photoelectron studies encompassing photoelectron diffraction as a complement to conventional photoelectron spectroscopy; high-resolution electron microscopy either alone or in association with electron-stimulated X-ray emission microanalysis; and neutron scattering techniques. In reviewing the principles, scope and application of these methods specific case histories are selected from representative minerals belonging to the serpentines, kandites, smectites, micas, vermiculites, chloritoids, zeolites and intergrowths of these with one another or with other silicate minerals. Emphasis is placed on problems not readily amenable to solution by traditional, X-ray based procedures.

## 1. Introduction

A wide variety of techniques has, over the years, been used to elucidate the structure of clay minerals and the various complexes, usually intercalates, that they form with organic guests. Many of these techniques are classical and rather indirect; some of the more recent, spectroscopic ones are less model-dependent – as far as interpretation is concernerned – than their traditional predecessors, but only a few yield information of a more or less direct kind. If good crystalline specimens are available, X-ray crystallography reigns supreme as the single, most powerful direct technique inasmuch as it generally affords unambiguous information pertaining to bond lengths, bond angles, site occupancies and coordination numbers. By their very nature, the majority of clay minerals, and almost invariably the chemically more interesting ones, are not well ordered, they are not stoichiometrically well behaved, and they are not crystallographically or compositionally pure. Clay minerals, more so perhaps than most other minerals, occur as coexistent species, there being (as we shall see later) often quite marked tendencies for intergrowths of different structure and composition to occur within one particular microscopic region of a specimen. X-ray crystallographic techniques are not, therefore, universally suited for the study of many clay minerals and their compounds.

In this paper we focus on four relatively new methods of probing the structure of clay minerals: high-resolution (magic-angle-spinning) nuclear magnetic resonance (n.m.r.); X-ray photoelectron studies; high-resolution electron microscopy; and neutron scattering studies. Each of these techniques has brought to light fresh insights into the nature of silicates in general (see Thomas *et al.* 1978–9; Thomas 1977, 1982*a*, *b*, 1983; Fyfe *et al.* 1983; Thomas 1979; Rae-Smith *et al.* 1979; Cheetham *et al.* 1982). Some of them have also shed new light on the structure, properties and behaviour of the very many intercalates formed, especially by smectites (montmorillonite and hectorite in particular), with organic guests (see Thomas 1982*b*; Pinnavaia 1983; Ballantine *et al.* 1983, 1984; Tennakoon *et al.* 1983). These organic

intercalates of clay minerals give rise to a rich diversity of chemical reactions (see Thomas 1982*b*; Pinnavaia 1983; Ballantine *et al.* 1983). An illustration of the importance of interlamellar protonation and interlamellar isomerization of carbocations formed by, for example, the addition of protons to alk-1-enes is given in schemes 1 and 2.

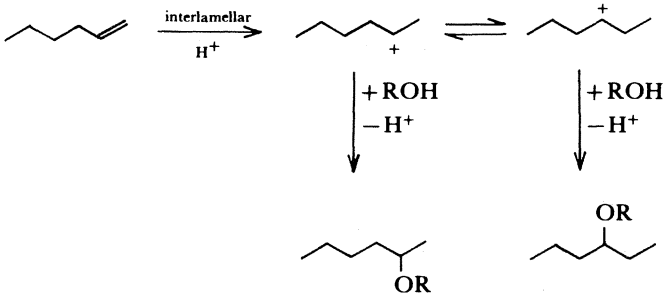


R = alkyl: hex-2-yl ether R = alkyl: hex-3-yl ether

R = H: hexan-2-ol R = H: hexan-3-ol

SCHEME 1

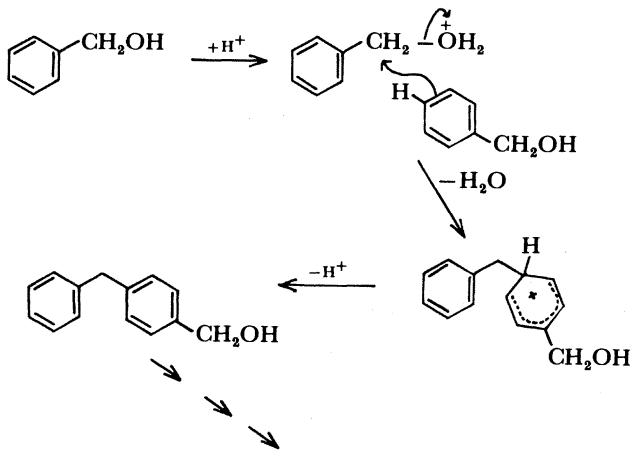


1,4- + 1,2-poly(phenylene–methylene)

$(CH_2–C_6H_4–CH_2–C_6H_4)_n$

SCHEME 2

## 2. HIGH-RESOLUTION SOLID-STATE NUCLEAR MAGNETIC RESONANCE

When molecules tumble freely, as they do in the isotropic liquid state, the associated n.m.r. absorption lines are very sharp because the broadening influences arising from dipolar and other interactions are averaged out by the motion of the dispersed species. Even with solid clay mineral catalysts, quite sharp $^{13}C$ and $^{1}H$ n.m.r. spectra can be obtained from intercalated entities provided the latter are in a more or less free state of rotational and translational motion in the interlamellar regions. Tennakoon *et al.* (1984) have shown how, using $^{13}C$ n.m.r., the course of a catalytic reaction taking place in the interlamellar environment may be traced. The proton-catalysed addition of water to 2-methyl-propene shown in scheme 3: yielding *t*-butanol is readily identified from the $^{13}C$ n.m.r. spectrum (figure 1).

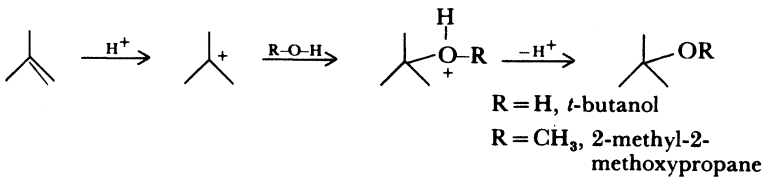


SCHEME 3

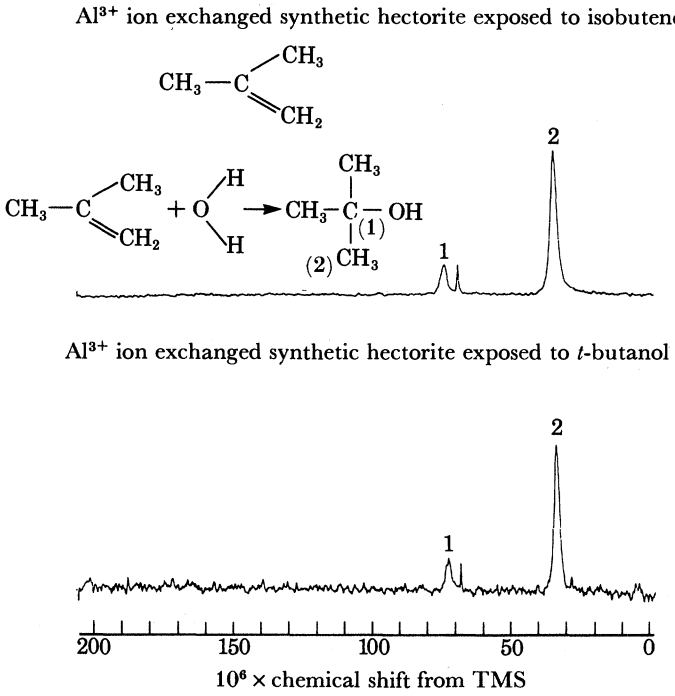


FIGURE 1. $^{13}C$ n.m.r. spectra showing that when 2-methyl propene (isobutene) is intercalated in a synthetic hectorite *t*-butanol is formed when the guest species reacts with the interlamellar water. The peaks labelled 1 and 2 refer to the two distinct types of carbon atom in the *t*-butanol.

So far as recording $^{27}Al$ and $^{29}Si$ n.m.r. spectra of clay minerals are concerned, however, it is necessary, in order to diminish by the necessary degree the considerable broadening influences brought about by the static, anisotropic dipolar and quadrupolar interactions, to resort to more sophisticated instrumental techniques. These sophisticated procedures have been reviewed by Andrew (1981), who, in 1958 was first responsible for introducing the principle of rapidly spinning the sample at the so-called magic-angle (54° 44′) to the magnetic field in order to produce high-resolution spectra. Reviews to the principles and application of this technique to aluminosilicate minerals have been given elsewhere (see Fyfe 1983; Fyfe *et al.* 1983).

The salient features of the magic-angle spinning n.m.r. (m.a.s.n.m.r.) technique in the context of clay mineralogy is that: (i) sixfold and fourfold coordination of Al and Si can be readily distinguished (see figure 2) by $^{27}Al$ and $^{29}Si$ m.a.s.n.m.r., respectively; (ii) non-crystalline (amorphous) or partially crystalline specimens are readily studied; (iii) time-dependent, solid-state phenomena are readily monitored (such as the distribution of Si and Al ions amongst eight distinct tetrahedral environments in annealed synthetic cordierite (see Fyfe *et al.* 1983),

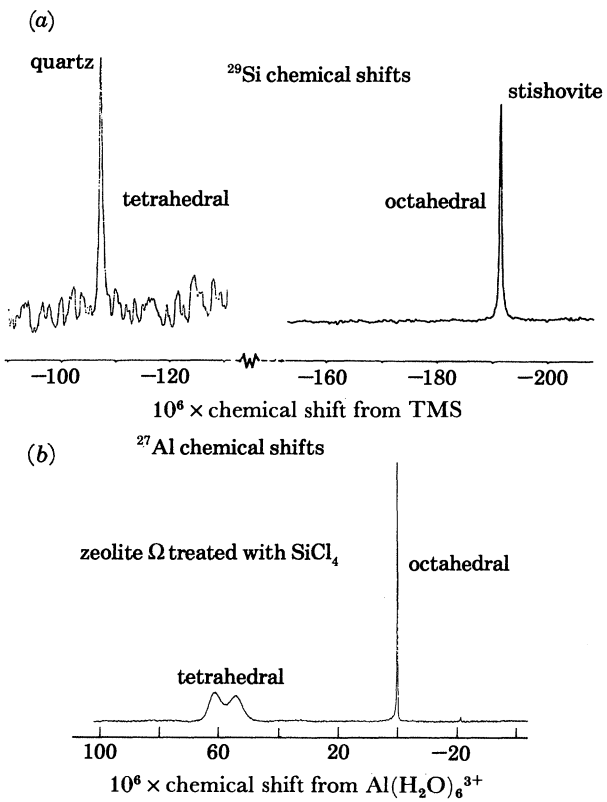


FIGURE 2*a*. $^{29}$Si m.a.s.n.m.r. spectra showing the very different chemical shift values for silicon in $SiO_2$ in which there is fourfold, tetrahedral coordination, as in quartz (left), and silicon in $SiO_2$ in which there is sixfold, octahedral coordination, as in stishovite (right). (After Thomas *et al.* 1983.) (*b*) $^{27}$Al m.a.s.n.m.r. spectrum of a dealuminated synthetic mazzite showing one sharp peak for an octahedral coordinated Al, and two broader peaks corresponding to two distinct tetrahedrally coordinated Al. (After Klinowski *et al.* 1983.)

TABLE 1. A SUMMARY OF SOME OF THE APPLICATIONS OF MAGIC-ANGLE-SPINNING N.M.R. IN THE STUDY OF ZEOLITIC MATERIALS

$^{29}$Si

1. Discriminates between $Si(OAl)_4$
   $Si(OAl)_3(OSi)$
   $Si(OAl)_2(OSi)_2$
   $Si(OAl)(OSi)_3$
   $Si(OSi)_4$
2. Distinct peaks are obtained for non-equivalent $Si(OSi)_4$ groupings.
3. Enables framework Si/Al ratios to be obtained, for example, in zeolites,

$$\frac{\mathrm{Si}}{\mathrm{Al}} = \sum_{n=0}^{n=4} I_{\mathrm{Si}(n\mathrm{Al})} \Big/ \sum_{n=0}^{n=4} \frac{n}{4} I_{\mathrm{Si}(n\mathrm{Al})}$$

   where $n$ is the number of Al atoms joined, via oxygen, to the central silicon. A similar equation holds for sheet silicates.
4. In dealuminated zeolites, the number of distinct $^{29}$Si peaks reflects the minimum number of non-equivalent Si sites in the unit cell.
5. A correlation exists between the chemical shift ($\delta$, measured in parts per million from TMS) and the average TOT angle ($\theta$ measured in degrees): $\delta = -25.44 - 0.5793\,\theta$.

$^{27}$Al

1. Readily distinguishes Al in fourfold from Al in sixfold coordination.
2. Combined with intensities of $^{29}$Si peaks, intensities of $^{27}$Al peaks enable framework Si/Al ratios to be determined when these are very large (*ca.* 10000).
3. In aluminosilicate catalysts, under favourable circumstances, enables a direct determination of active sites (that is, when synonymous with Al sites in framework) to be determined.

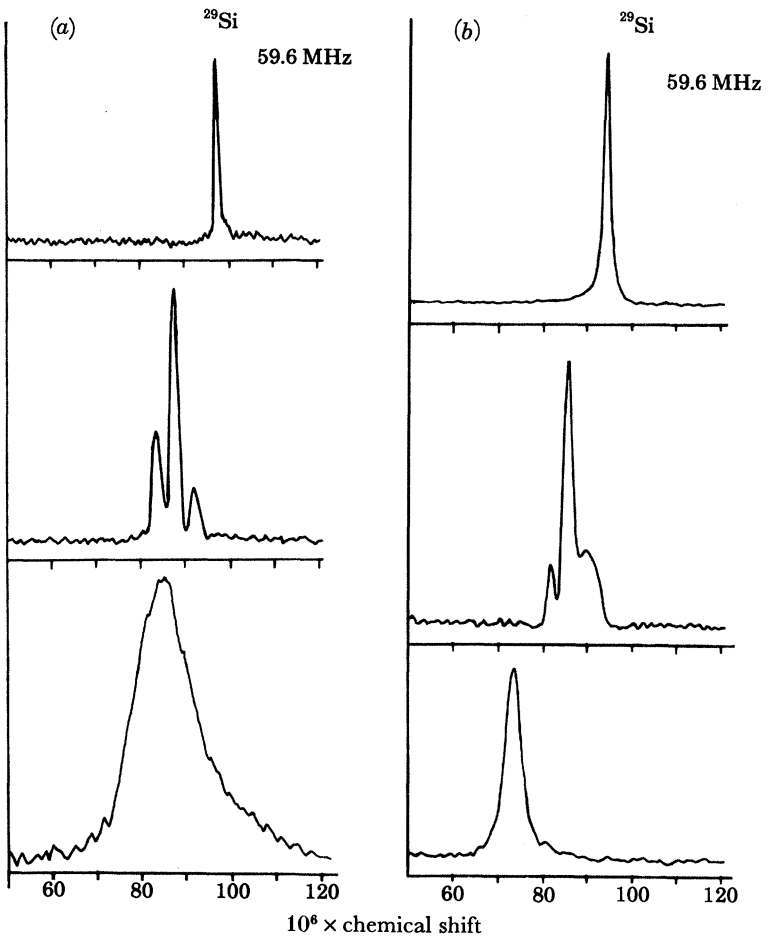


FIGURE 3. $^{29}$Si m.a.s.n.m.r. (at 59.6 MHz, that is, a $^1$H resonance of 300 MHz) of (*a*) talc, and two phlogopite samples one (P18) containing more magnetic impurities than the other (P8); and of (*b*) pyrophillite, muscovite and margarite. (After Sanz *et al.* 1984.) See text.

and (iv) in general, samples rich in paramagnetic or ferromagnetic constituents are not amenable to study because of unacceptably large line-broadening effects.

The power of m.a.s.n.m.r. in aluminosilicate chemistry, more particularly in characterizing zeolites, to which the $^{27}$Al and $^{29}$Si variants of this technique have so far been largely applied, is summarized in table 1. And the results of Sanz *et al.* (1984) and from our own studies (figures 3 and 4) show how promising $^{27}$Al and $^{29}$Si m.a.s.n.m.r. spectroscopy is likely to be so far as probing non-ferruginous samples of clay minerals is concerned. Serratosa's work (1984) has already shown how, using the procedures and equations employed in zeolite research (see Thomas *et al.* 1982; Klinowski *et al.* 1982) to evaluate Si/Al ratios and to test various models for Si, Al ordering, useful insights into the distribution of Al in the tetrahedral manifold of micas can be gained. What remains a little puzzling at present is the magnitude of the ratio of Al in tetrahedral and octahedral sites in, say, phlogopite. More exploratory work on, for example, differences in relaxation times and their influence upon peak intensities, is needed before we can gauge the trustworthiness of the m.a.s.n.m.r. technique as a general tool in clay

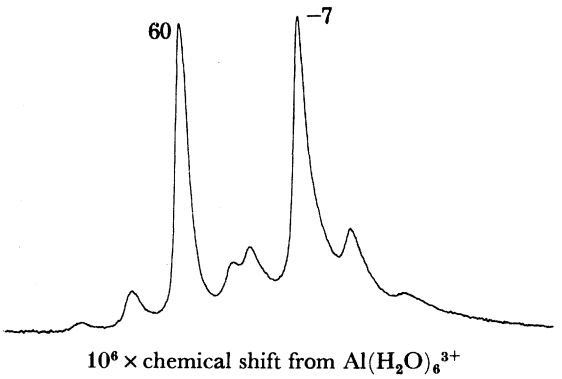


FIGURE 4. $^{27}Al$ m.a.s.n.m.r. spectrum at 104.3 MHz showing, at $60/10^6$, a peak from tetrahedrally coordinated, and, at $-7/10^6$, a peak from octahedrally coordinated Al in muscovite. Other, subsidiary peaks are spinning side-bands of the major peaks.

mineralogy. What is already apparent, however, is its great utility in probing local environments in precursor gels (see Thomas *et al.* 1983; Engelhardt *et al.* 1983).

### 3. X-RAY INDUCED PHOTOELECTRON STUDIES

There are two aspects to the study of clay minerals by photoelectrons liberated by means of irradiation with soft, but monochromatic X-rays. It is well known that $MgK_\alpha$ ($h\nu = 1253$ eV) or $AlK_\alpha$ ($h\nu = 1486.6$ eV) X-rays will, according to the Einstein photoelectric equation, yield electrons possessing well-defined kinetic energies (Adams *et al.* 1972). Knowing the photoelectric cross sections of the various core levels (Evans *et al.* 1978) and escape depths of the various photoemitted electrons (Adams *et al.* 1977), it is possible to relate the intensity of peaks such as those shown in figure 5 to quantitative measures of the elements present in a sample. The first aspect, therefore, is simply to record the X-ray induced photoelectron spectrum.

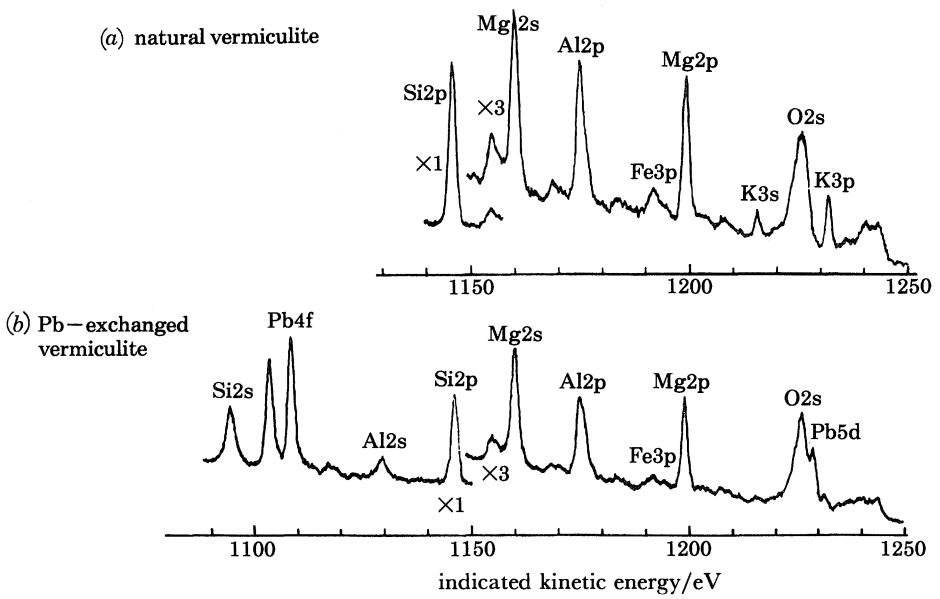


FIGURE 5. X.p.s. spectra of (*a*) natural and (*b*) lead-exchanged vermiculites (see text).

In figure 5*b*, for example, we see how well this X-ray induced photoelectron spectroscopic procedure (often called X.p.s. or electron spectroscopy for chemical analysis (e.s.c.a.)) detects the cation exchange that takes place when naturally occurring vermiculite is exposed to a warm aqueous solution of $Pb^{II}$-containing ions. The disappearance of the $K_{3s}$ and $K_{3p}$ signals and the appearance $Pb_{4f}$ peaks are noteworthy features which readily stand out in figure 5.

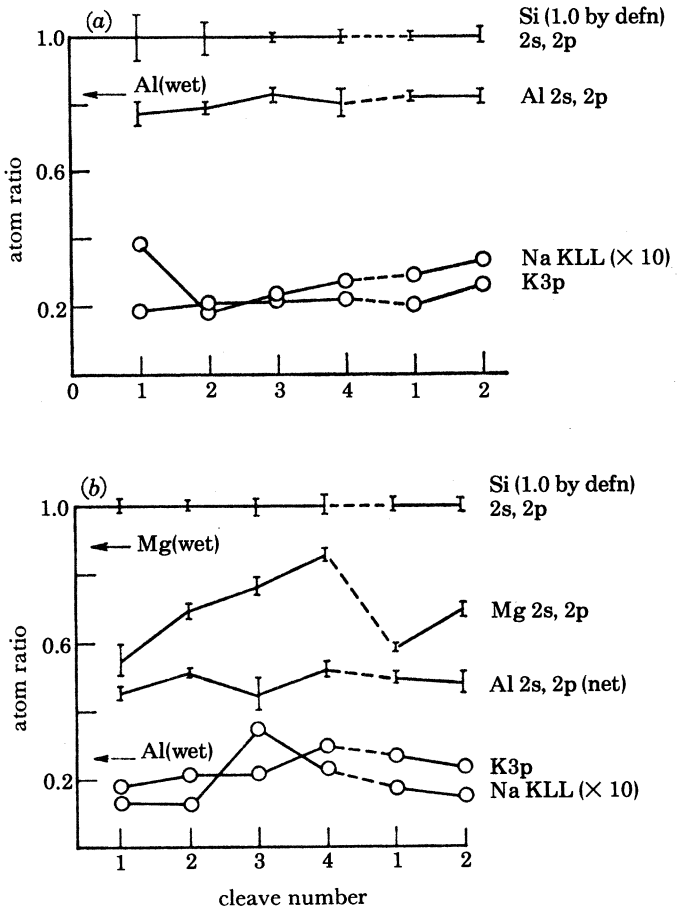


FIGURE 6. Variation in chemical composition over macroscopic distances as revealed by X.p.s. peak intensity ratios measured at a fixed take-off angle (see figure 7 and text). The numerals on the abscissa relate qualitatively to depth: the first four cleaves in each case were taken over about 1 mm of the crystal. All cleavages were performed *in vacuo*. Bulk analyses for Mg and Al are indicated by the word 'wet', with arrows, in each plot: (*a*) muscovite, (*b*) phlogopite. (After Evans *et al.* 1979.)

When rather large single-crystal specimens of sheet silicates are available (e.g. muscovite and phlogopite) it is relatively straightforward to carry out successive cleavage, *in situ*, inside the sample chamber of the X-ray photoelectron spectrometer (see Evans *et al.* 1979) so that detailed surface compositional analyses (to a depth of approximately 4–10 nm below the exposed cleavage-face) can be carried out by X.p.s. measurements following successive acts of cleavage (see figure 6). What is noticeable here is that, whereas the composition of successive exposed surfaces of muscovite agree well with one another, and with the average bulk composition, for surfaces of phlogopite there are significant variations one with respect to the other and with respect also to the mean composition of the bulk specimen. The magnesium content

is particularly different at each cleavage surface from that of the bulk and so, but to a rather lesser degree, is the aluminium content of phlogopite.

### (*a*) *X-ray photoelectron diffraction* (*X.p.d.*)

In this technique, which constitutes the second aspect of the study of clay minerals by photoelectrons, one monitors the 'diffraction' of the X-ray induced photoelectrons as a function of the take-off angle of the emitted electron. Although the existence of such diffraction has been known for some time (see Siegbahn *et al.* 1970), its use as a tool for structural elucidation of the near-surface regions of solids is quite recent (Adams *et al.* 1978; Evans *et al.* 1979; Thomas 1979; Evans *et al.* 1979). To illustrate the principles of the technique, consider the

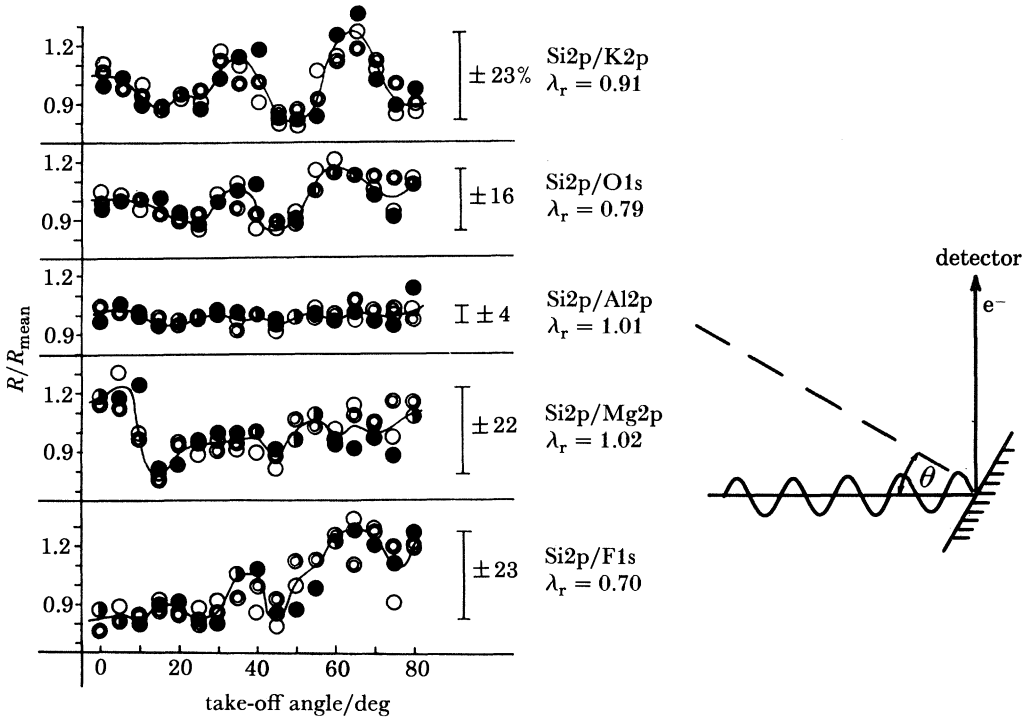


FIGURE 7. Schematic illustration of orientation of crystal and the set-up required to record X.p.d. spectra (see text). The X.p.d. patterns for phlogopite (where three cleaves in the same orientation are distinguished by single circles, double circles and solid circles) show that Si and Al atoms in this silicate are in essentially identical crystallographic environments, since there is little variation in intensity ratio with take-off angle.

variation of the intensity of the $Si_{2p}$ photoemitted electrons of phlogopite mica as a function of take-off angle. The intensity will fluctuate because of the multiple diffraction that the electrons experience between the region where they are generated (inside the crystal) and the region where they escape (at the exterior surface) into the vacuum and into the electron spectrometer (the setting of which is fixed so as to register, in this case, $Si_{2p}$ photoelectrons only). If, as is generally supposed, $Al^{3+}$ ions occupy some of the tetrahedral sites normally taken up by $Si^{4+}$, then the angular variation of $Al_{2p}$ and $Si_{2p}$ photoelectrons should be identical, a situation which would not hold good for a mineral in which $Al^{3+}$ is preferentially resident in octahedral sites. (There are a few other subtleties that have to be considered in a rigorous treatment of the factors governing angular variation in intensity of photoemission; see Evans *et al.* (1979), for a full discussion.)




PHILOSOPHICAL TRANSACTIONS OF THE ROYAL SOCIETY A MATHEMATICAL, PHYSICAL & ENGINEERING SCIENCES

Figure 7, which has, as an inset, a diagrammatic representation of the experimental set-up required to record X-ray photoelectron diffractograms, shows that, in phlogopite, there is indeed accommodation of the $Al^{3+}$ in the tetrahedral manifold. (Ratios of intensity such as $Si_{2p}/Al_{2p}$ constitute a more reliable and useful means of plotting these diffractograms: instrumental and other difficulties are largely compensated in this fashion.) Note that, for two elements (such as Si and K) which are separately confined to unique and different crystallographic sites, the ratio of their photo-peak intensities exhibit maximal variation with take-off angle (see the $Si_{2p}/K_{2p}$ variation in figure 6).

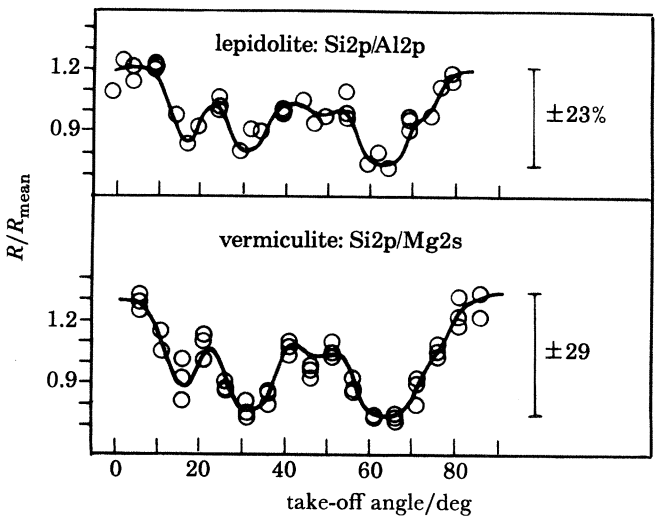


FIGURE 8. X.p.d. patterns for the major tetrahedrally (that is, Si and Al) and octahedrally (Al, Mg) coordinated elements in (*a*) lepidolite and (*b*) vermiculite.

By using procedures of this kind it has been shown that $Al^{3+}$ ions in lepidolite and $Mg^{2+}$ ions in vermiculite are in identical crystallographic environments, both being situated at octahedral sites (figure 8) other useful information to emerge from X.p.d. measurements on clay minerals are that $Na^{+}$ ions present in muscovite in quantities too small to be detected by conventional X-ray methods (see Brown, this symposium), occupy sites that are similar, but not quite equivalent, to those occupied by the interlamellar ions for which they substitute; and that the degree of hydration of exchangeable cations in clay minerals can be ascertained. Thus, whereas interlamellar $Ca^{2+}$ and $Pb^{2+}$ ions in weathered or solution-treated vermiculite are hydrated, interlamellar $K^{+}$ ions are not. X.p.d. measurements have so far been restricted to those clay minerals that occur as rather large crystals. There is no reason why this technique can also be applied to much smaller specimens provided the necessary instrumental modifications and improvements in detection of photoelectrons (both already feasible) are made.

## 4. High-resolution electron microscopy

The principles and practical considerations relating to the use of this powerful technique for the study of silicate minerals in general and for clay minerals in particular have been previously described (see Thomas *et al.* 1978–9, 1982; Thomas 1980, 1982, 1983; Millward & Thomas 1982; Beer *et al.* 1981; Jefferson *et al.* 1981). Briefly, very thin specimens are examined and the

image is recorded at several, so-called defocus settings and also using several thicknesses in the range 5–50 nm. Methods are available for the calculation of the expected image contrast for a given supposed structure. The trustworthiness of a supposed model structure is assessed according to its degree of matching with the observed image using several thicknesses and several defocus settings. If possible, also, the matching operation between observed and calculated image is carried out employing as many different crystallographic projection directions as possible. For the anisotropic clay minerals it is generally much better to record images in directions that lie along the layer planes. Although this is, in practice, not easy; since appropriate fractured, or ion-beam thinned specimens can be produced only with some difficulty, more discriminating, interpretable and less ambiguous, images are thus obtained. Occasionally, however, as with the serpentines (see below), valuable information can be obtained by imaging in directions perpendicular to the layer planes. (For a summarizing account of the especial merit of high-resolution electron microscopy (h.r.e.m.), which produces real-space images, in the structural elucidation of minerals containing light elements, see Pring *et al.* (1983), who describe the matching of calculated and observed images along all three principal, high-symmetry directions in the mineral rhodizite.)

One of the supreme advantages of h.r.e.m. in the study of silicate minerals is that it records, in real-space, the presence and extent of structural intergrowths. Much valuable information pertaining to zeolites, both faujasitic (Millward & Thomas 1982) and the synthetic ones known as pentasils, that is, ZSM-5 and ZSM-11 (see Millward & Thomas 1982*b*; Thomas *et al.* 1983), can be obtained in this way. New types of boundaries including those known as coincidence boundaries (Terasaki *et al.* 1984) have been found in other zeolitic structures where there are one-dimensional tunnels, as in zeolite L.

### (*a*) *The study of serpentine minerals: their microstructure and polymorphism*

There are three forms of serpentine (ideal formula $Mg_3Si_2O_5(OH)_4$): lizardite, which has a platy morphology; chrysotile, which is tubular; and antigorite, which is also platy but corrugated (see figure 9). All three polymorphs tend to coexist with one another. All are made up of layers separated by *ca.* 0.7 nm, the components of which are a two-dimensional sheet of corner-linked $SiO_4$ tetrahedra, and, coherently attached to this sheet; a two-dimensional network of $Mg(O, OH)_6$ edge-sharing octahedra. The upper vertices of the $SiO_4$ tetrahedra are linked as shown in figure 9, to the $Mg(O, OH)_6$ octahedra: some of the oxygens are common to both networks.

Chrysotile is tubular, so it is argued, because the ideal (Mg-containing) octahedral sheet is too large to enmesh exactly with the adjoining $SiO_4$ sheet. Hence, the tubular morphology is adopted because, in this way, the structure can neatly accommodate the larger radius of curvature of the outer octahedral layer as well as the smaller curvature of the inner tetrahedral layer.

It has been possible to test the hypothesis that, by substituting Al for Mg in octahedral sites and, or, Al for Si in tetrahedral sites, the dimensions of the octahedral sheets can then be equalized with those of the tetrahedral ones. Combined h.r.e.m. and energy-dispersive X-ray emission microanalysis confirms that, in chrysotile there is no aluminium (figure 10, plate 1). The situation is essentially the same in antigorite where a corrugated structure (figure 9) is adopted as an alternative to the tubular one so as to accommodate the discrepant dimensions of the contiguous octahedral and tetrahedral sheets. The flat, platy lizardite does indeed contain

aluminium, and it has been shown by Crawford *et al.* (1978), that 16% of the Mg in octahedral sites and 12% of the Si in tetrahedral sites are replaced by Al. Note that, in the high-resolution image of antigorite, the postulated 'corrugated' structure of, with its long wavelength periodicity of *ca.* 43 nm is directly visible, as is the 0.46 nm unit-cell repeat distance.

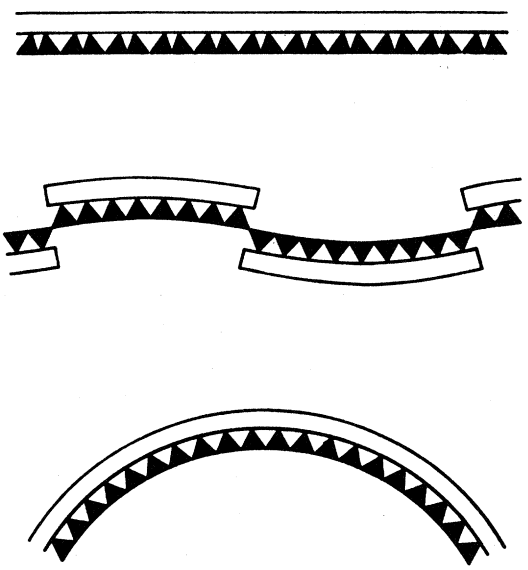

FIGURE 9. Schematic illustration of the morphological features of the serpentine minerals: chrysotile (bottom), antigorite (middle) and lizardite (top). The tetrahedral ($SiO_4$) layer is shaded and the octahedral sheet (Mg(O, OH)) or Mg, Al(O, OH) is left unshaded, for clarity.

In an elegant h.r.e.m. study of the serpentine minerals (from the Cascade Mountains, Washington, U.S.A., and from Ocna de Fier, Romania) Veblen & Buseck (1979) found, intimately, intergrown within each other the serpentine minerals chrysotile, lizardite and antigorite as well as talc, chlorite and amphibole. They also found evidence for mixed-layer silicate consisting of serpentine and talc layers.

### (*b*) *The study of chloritoid: an unusual layer silicate*

This silicate (idealized formula $(Mg_1Fe)_2Al(Al_3Si_2O_{10})(OH)_4$) consists of two kinds of quite complicated sheets; and the several polytypic forms of the mineral arise from the various possible stacking sequences of these component sheets. It so happens that specimens of chloritoid are rather readily prepared for h.r.e.m. studies because it possesses a cleavage perpendicular to the basal plane (see Jefferson & Thomas 1978) which make it readily possible for the stacking of the sheets to be directly recorded.

Three main points emerge from the h.r.e.m. study of chloritoid. First, two new polytypes were discovered, one of monoclinic the other of triclinic symmetry. Figure 11, plate 2, shows a typical example of the way in which the various polytypes intergrow coherently with one another: four of the known five polytypes of chloritoid can be seen to coexist in a small region of one sample. All these polytypes (the $2M_1$, $2M_2$ monoclinic variants and the 1Tc 3Tc triclinic variants) were all 'encountered' in the h.r.e.m. study of Jefferson & Thomas (1979*a*) in traversing a distance of *ca.* 50 nm.

Secondly, just as with other silicate minerals, notably the chain silicates typified by the

pyroxenoids such as wollastonite, rhodonite and pyroxmangite, it has been found that polytypic strips can terminate within others, thereby creating local structural discontinuities which are likely to function both as centres of preferential chemical attack and as points of mechanical weakness. Thirdly, energy dispersive X-ray emission microanalysis, down to volumes of *ca.* $10^7$–$10^8$ nm$^3$, show no correlation between elemental composition and the particular polytype peculiar to the region in question. In the course of a microscopic study of topotactic dehydration of chloritoid (Jefferson & Thomas 1979*b*) it emerged that there could be a correlation between a given polytype and the oxidation state of the Fe ions present in the clay mineral.

### (*c*) *Exsolution and the crystal chemistry of the recently discovered mica mineral wonesite*

In a very recent study, Veblen (1983*a*) has demonstrated well the merit of h.r.e.m. as a tool in clay mineral research. He has focused attention on the sodium mica wonesite from the Post Pond Volcanics, Vermont, and has discovered the first known example of exsolution in a mica. It transpires that the wonesite (see Spear *et al.* (1981) for a description of this new rock-forming silicate) exsolves partially into a lamellar intergrowth of talc and a sodium mica having fewer interlayer site vacancies than the initial wonesite. The mica is found to be enriched in Na, Al, K, Ti, Cr and Fe relative to the talc. The lamellae, the wavelength of which varies from tens of nanometres to about 0.5 μm, are inclined to the layers of the mica and talc structures at a variable angle that averages about 37° (that is, about a third of the tetrahedral angle). This microstructure explains why wonesite is not expandable in water, in contrast to the behaviour of many synthetic and naturally occurring intergrowths of smectites and micas. A schematic illustration of the exsolved structure, along with the low-resolution electron micrograph on which it is based is shown in figure 12.

From Veblen's h.r.e.m. studies (Veblen 1983*b*) of the microstructures and mixed layering in intergrown wonesite, chlorite, talc, biotite and kaolinite, several noteworthy features emerge. The chlorite occurs in intergrown one-layer and disordered polytypes; the wonesite occurs in one-layer, two-layer, three-layer and disordered forms, and the biotite occurs as one-layer and two-layer polytypes with minor stacking disorder. Some of the wonesite also exhibits turbostratic stacking, of the kind that is common in incompletely crystallized specimens of graphite. Parts of the chlorite exhibit perfect alternation of the talc-like and brucite-like layers. Likewise, occasional brucite-like layers are found in most of the wonesite (see figure 13, plate 3). In both chlorite and wonesite, these extra layers are in some cases observed to terminate (compare chloritoid described in (*b*) above). In some places, the chlorite and mica structures intergrow freely, either in almost total disorder or as slabs of chlorite and mica up to tens of nanometres thick. Thin slabs of kaolinite, talc and potassium biotite also intergrow with the chlorite and wonesite. The mixed layering phenomena in this specimen demonstrates that chlorite which appears normal in thin section can occasionally deviate substantially from ideal chlorite stoichiometry.

---

## Description of plate 1

Figure 10. High-resolution electron microscopy micrographs and X-ray emission spectra of serpentines: (*a*) lizardite, (*b*) antigonite, showing the corrugation periodicity of *ca.* 4.3 nm, and (*c*) chrysotile, showing the interlayer spacing (0.74 nm).





PHILOSOPHICAL TRANSACTIONS OF THE ROYAL SOCIETY A MATHEMATICAL, PHYSICAL & ENGINEERING SCIENCES

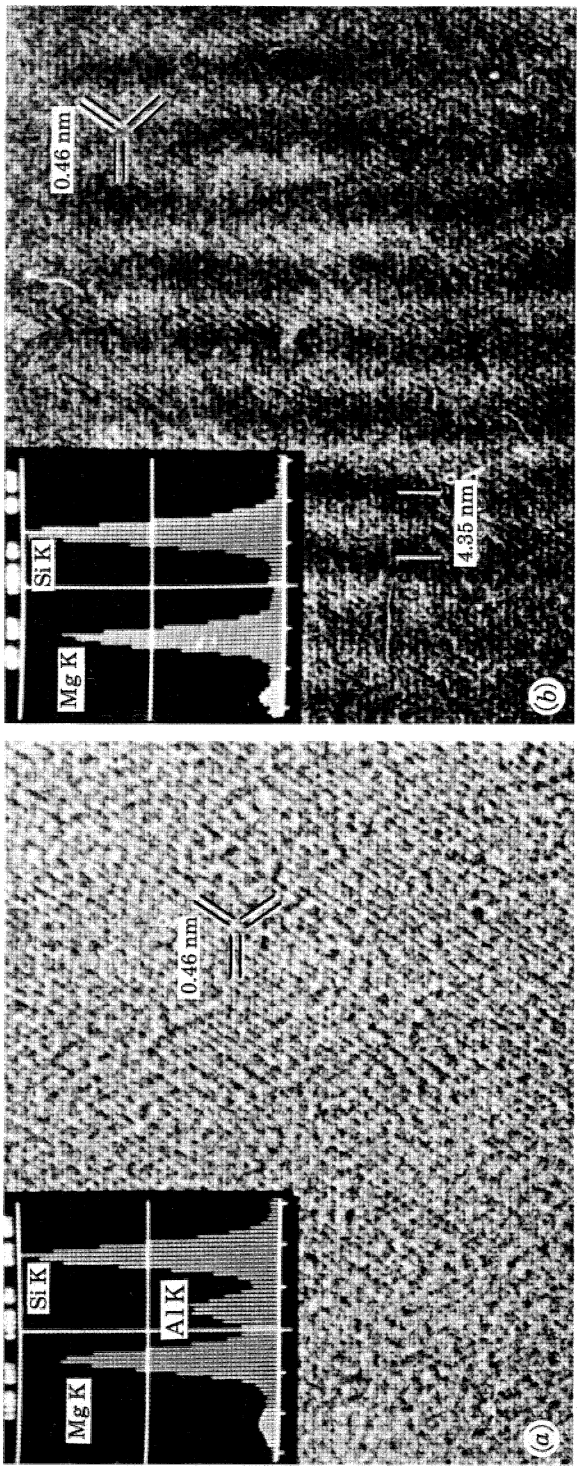


(*Facing p.* 282)



PHILOSOPHICAL TRANSACTIONS OF THE ROYAL SOCIETY A MATHEMATICAL, PHYSICAL & ENGINEERING SCIENCES

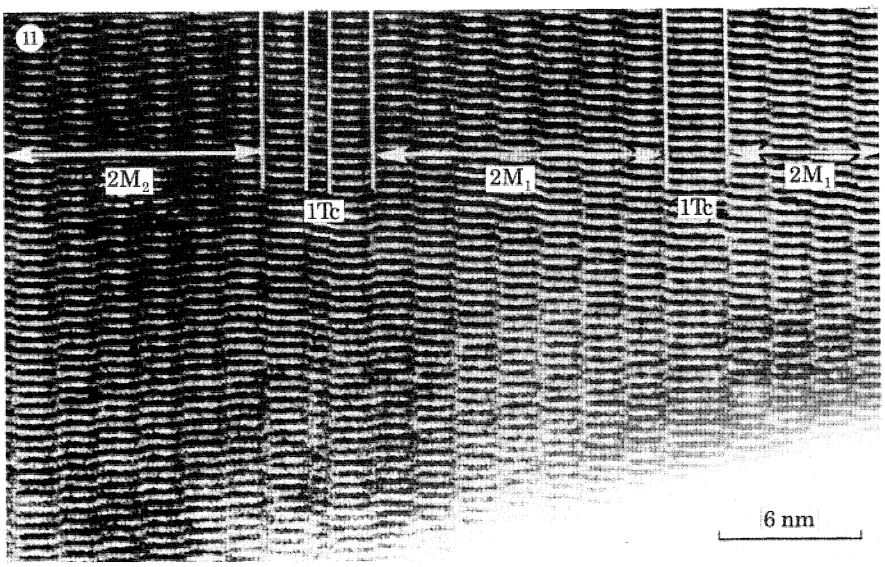


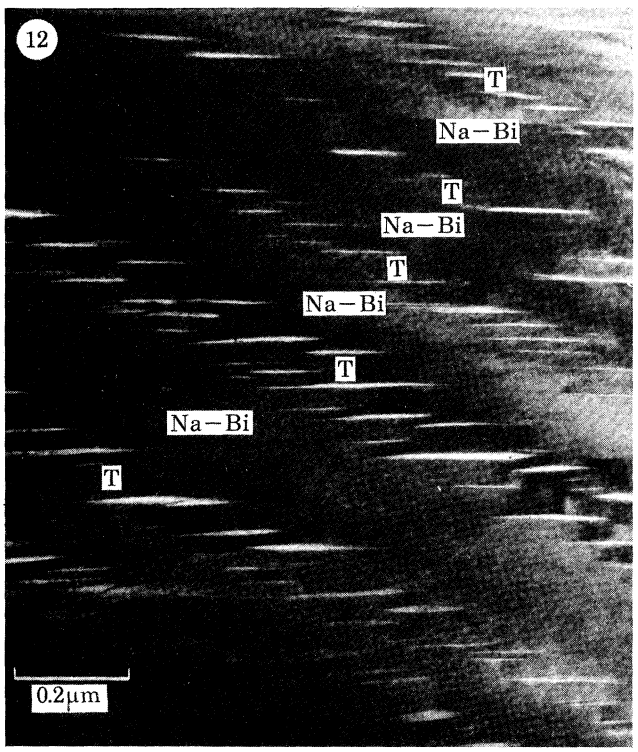


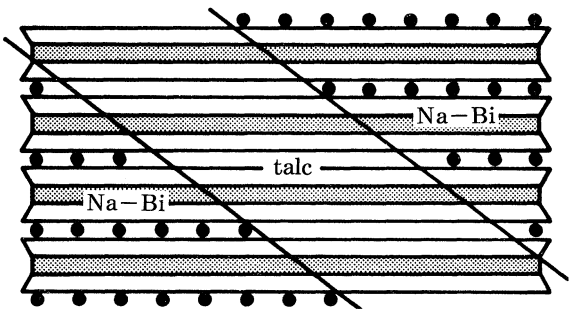


FIGURES 11 AND 12. For description see opposite.



PHILOSOPHICAL TRANSACTIONS OF THE ROYAL SOCIETY A MATHEMATICAL, PHYSICAL & ENGINEERING SCIENCES

## Description of plate 2

Figure 11. High-resolution electron microscopic image of a thin section of chloritoid showing intergrowths of various polytypes (see text).

Figure 12*a*. Low-resolution bright-field electron micrograph of the lamellar microstructure in wonesite. Talc (T) and sodium biotite (Na–Bi) lamellae are titled with respect to the plane (001), which is horizontal. The talc lamellae can be recognized by the white, lenticular voids parallel to (001). (*b*) Schematic drawing of this microstructure, emphasizing that the lamellae are not parallel to the structural layers. Circles represent interlayer alkali sites. (After Veblen 1983*a*.)

PHILOSOPHICAL TRANSACTIONS OF THE ROYAL SOCIETY A MATHEMATICAL, PHYSICAL & ENGINEERING SCIENCES

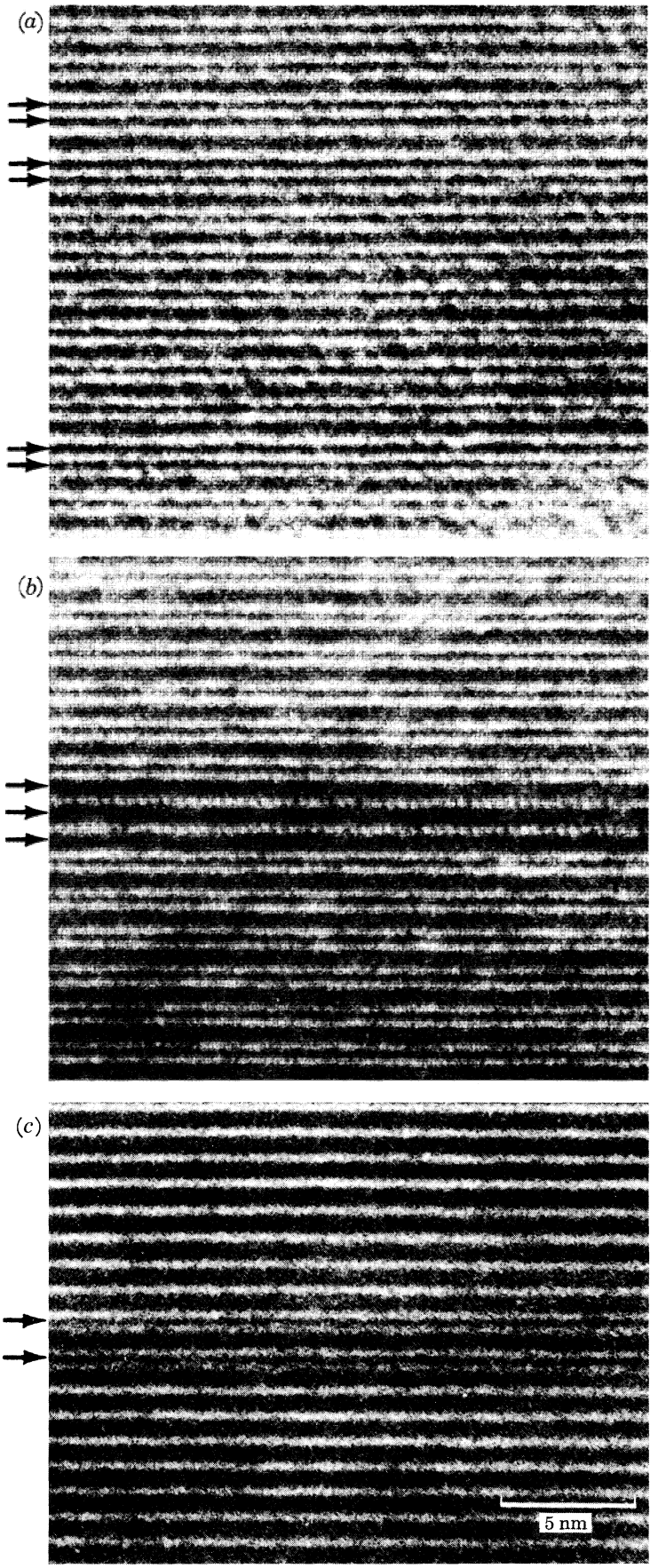


FIGURE 13. For description see opposite.



PHILOSOPHICAL TRANSACTIONS OF THE ROYAL SOCIETY A MATHEMATICAL, PHYSICAL & ENGINEERING SCIENCES

The unusual material designated 'poorly crystallized material' abundant in Mighei $CM_2$ carbonaceous chondrite (see Fuchs *et al.* 1973) has recently been shown by Tomeoka & Buseck (1983), using h.r.e.m., to be largely composed of a Fe–Ni–S–O layered mineral which occurs in coherent intergrowths with smectites in various ordered and disordered sequences.

### (*d*) *Other possibilities*

Already it has proved possible to image some of the pillared clays (otherwise known as cross-linked smectites) which are proving to be so promising as catalytic agents intermediate in their performance between zeolites on the one hand and clay minerals on the other (see Vaughan & Lussier 1980; Vaughan 1984; Thomas 1982*b*). Imaging of this kind by h.r.e.m. should shed much light on the structure and properties of this new class of novel, pillared catalysts, in which the pillars themselves can be rich in aluminium oxide, or gallium oxide or zirconium (as well as other metal) oxides. So far as the micas themselves are concerned, Iijima & Buseck (1978) and Iijima & Zhee (1982) have shown the value of h.r.e.m. as a tool for structural characterization.

## 5. Neutron scattering

Most clay minerals exhibit a high degree of preferred orientation parallel to the layer planes. This being so it is readily possible, using appropriately mounted thin films of the minerals, to obtain (00*l*) reflections from X-rays or neutrons up to very high order (for example, $l = 16$). This, in turn, yields one-dimensional Fourier plots of nuclear scattering density of the constituent atoms in the framework as well as of the ions in the interlamellar regions of the clay mineral in question (see Thomas *et al.* 1976; Adams *et al.* 1976).

For the study of intercalates, including time-dependent monitoring of transformations from 3-layer to 2-layer to 1-layer intercalates of organic guests (Adams *et al.* 1977), this approach has been of considerable value. The subtle changes in orientation of, for example, tetrahydrofuran in proceeding from $Ni^{2+}$-exchanged to $Co^{2+}$-exchanged montmorillonite can be readily followed in this way (see Thomas *et al.* 1976). So also can the positions of hydrogen atoms in the kaolinite: formamide intercalate (Adams *et al.* 1976).

A quite different kind of neutron-based study of aluminosilicates is also possible. This entails the so-called Rietveld powder profile method in which, using routines described fully elsewhere (see Stewart 1978; Rae-Smith *et al.* 1979), the atomic coordinates and occupancy factors for a powdered (but ordered) structure is evaluated by minimizing the differences between observed and computed (on the basis of the refined structure) profiles for the neutron-diffractogram.

This approach has been particularly successful for various cation-exchanged zeolites (Cheetham *et al.* 1982; Cheetham *et al.* 1983) – see figure 14. Si–O and Al–O bond distances within the zeolite framework can be reliably extracted using this technique. Recently evidence has been obtained, using the Rietveld method, to suggest that in dealuminated faujasitic zeolites

---

### Description of plate 3

Figure 13. Mixed layering defects. (*a*) Extra brucite-like layers (or missing talc-like layers) in chlorite. The arrows indicate pairs of adjacent brucite-like layers. (*b*) Extra talc-like layers in chlorite (or missing brucite-like layers). The arrows indicate three adjacent talc-like (TOT) layers. (*c*) Brucite-like layers (arrowed) intercalated in wonesite.





PHILOSOPHICAL TRANSACTIONS OF THE ROYAL SOCIETY A MATHEMATICAL, PHYSICAL & ENGINEERING SCIENCES

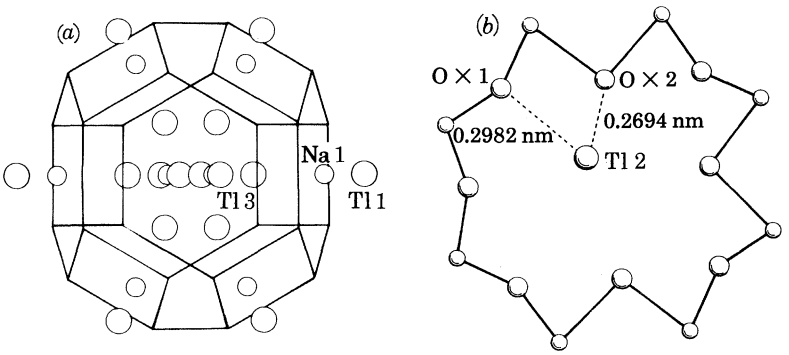


FIGURE 14. The location of the exchangeable cations $Na^+$ and $Tl^+$ in zeolite A. (*a*) The Tl(1), Tl(3) and Na(1) sites and their closeness to the six-membered face of the β-cage are emphasized. (*b*) Location of Tl(2) in the so-called eight-ring aperture. (After Cheetham *et al.* 1982.)

$AlO_4^{5-}$ units are arranged, in an ordered fashion within the so-called β-cages (sodalite cages). (G. D. Stucky, personal communication.)

In those clay minerals where crystallographic order is well-developed (that is, in those that have already been amenable to X-ray crystallographic techniques) there is every prospect that the Rietveld neutron profile method (or indeed, its more recently developed X-ray Rietveld method) will prove to be an important additional structural tool especially in that the method dispenses with the need to obtain single-crystal specimens.

I acknowledge with gratitude support from the S.E.R.C. and the University of Cambridge.

## REFERENCES

Adams, J. M., Evans, S., Reid, P. I., Thomas, J. M. & Walters, M. J. 1977*a* *Analyt. Chem.* **49**, 2001.
Adams, J. M., Evans, S. & Thomas, J. M. 1978 *J. Am. Chem. Soc.* **100**, 3260.
Adams, J. M., Lukawski, K. S., Reid, P. I., Thomas, J. M. & Walters, M. J. 1977*b* *J. chem. Res.* (*M*) 0301.
Adams, J. M., Reid, P. I., Thomas, J. M. & Walters, M. J. 1976 *Clays Clay Miner.* **24**, 267.
Adams, I., Thomas, J. M. & Bancroft, G. M. 1972 *Earth Planet Sci. Lett.* **16**, 429.
Andrew, E. R. 1981 *Int. Rev. phys. Chem.* **1**, 195.
Bailey, S. W. 1983 *Clay minerals* (ed. G. Brown and G. W. Brindley). Mineralogical Society.
Ballantine, J. A., Purnell, J. H. & Thomas, J. M. 1983 *Clay miner.* (In the press.)
Ballantine, J. A., Purnell, J. H. & Thomas, J. M. 1984 *J. Molec. Catalysis.* (In the press.)
Beer, M., Carpenter, R. W., Lyman, C. E., Eyring, L. E. & Thomas, J. M. 1981 *Chem. Eng. News* **59**, 40.
Cheetham, A. K., Eddy, M. R., Jefferson, D. A. & Thomas, J. M. 1982*a* *Nature, Lond.* **299**, 24.
Cheetham, A. K., Eddy, M. R., Jefferson, D. A. & Thomas, J. M. 1982*b* *Nature, Lond.* **299**, 924.
Cheetham, A. K., Eddy, M. R., Klinowski, J. & Thomas, J. M. 1983 *J. chem. Soc. chem. Commun.* 23.
Crawford, E. S., Jefferson, D. A., Thomas, J. M. & Bishop, A. C. 1978 *J. chem. Soc. chem. Commun.* 986.
Engelhardt, G., Fahlke, B., Magi, M. & Lippmaa, E. 1983 *Zeolites* **3**, 292.
Evans, S., Adams, J. M. & Thomas, J. M. 1979 *Phil. Trans. R. Soc. Lond.* A **292**, 563.
Evans, S., Raftery, E. & Thomas, J. M. 1978 *Surface Sci.* **89**, 64.
Fyfe, C. A. 1983 In *Inorganic chemistry: towards the 21st century* (ed. M. H. Chisholm), p. 405. A.C.S. Symposium series, no. 211. Washington D.C.: American Chemical Society.
Fyfe, C. A., Gobbi, G., Klinowski, J., Putnis, A. & Thomas, J. M. 1983 *J. chem. Soc. chem. Commun.* **23**, 556.
Fyfe, C. A., Thomas, J. M. & Lyerla, J. R. 1981 *Angew. Chem.* **20**, 96.
Hewat, A. W. 1978 Powder Rietveldt and refinement system (I.L.L. Grenoble Report). Grenoble: I.L.L.
Iijima, S. S. & Buseck, P. R. 1978 *Acta Cryst.* A **34**, 709.
Iijima, S. S. & Zhu, J. 1982 *Am. Miner.* **67**, 1195.
Jefferson, D. A. & Thomas, J. M. 1978 *Proc. R. Soc. Lond.* A **361**, 399.
Jefferson, D. A. & Thomas, J. M. 1979 *Acta. Cryst.* A **35**, 416.
Jefferson, D. A., Thomas, J. M. & Egerton, R. 1981 *Chemy Brit.* **17**, 514.
Jenkins, H. D. B. & Hartman, P. 1982 *Phil. Trans. R. Soc. Lond.* A **304**, 397.




PHILOSOPHICAL TRANSACTIONS OF THE ROYAL SOCIETY A MATHEMATICAL, PHYSICAL & ENGINEERING SCIENCES

Klinowski, J., Anderson, M. W. & Thomas, J. M. 1983 *J. chem. Soc. chem. Commun.* 525.
Klinowski, J., Ramdas, S., Thomas, J. M., Fyfe, C. A. & Hartman, J. S. 1982*b* *J. Chem. Soc., Faraday Trans. II.* **78**, 1025.
Klinowski, J., Thomas, J. M., Fyfe, C. A. & Gobbi, G. 1982*a* *Nature, Lond.* **296**, 533.
Millward, G. R. & Thomas, J. M. 1983 In *Surface properties and catalysis by non metals and oxides* (ed. J. P. Bonelle), p. 197. Proc. NATO Advanced Study Institute. Dordrecht: D. Reidel.
Pinnavaia, T. J. 1983 *Science, Wash.* **220**, 365.
Pring, A., Jefferson, D. A. & Thomas, J. M. 1983 *J. chem. Soc. chem. Commun.* 734–736.
Rae-Smith, A. R., Cheetham, A. K. & Skarnulis, A. J. 1979 *J. appl. Cryst.* **12**, 485.
Sanz, J., Förster, H. G. & Serratosa, J. M. 1984 *Nature, Lond.* (In the press.)
Siegbahn, K., Gelius, U., Siegban, P. & Olson, D. 1977 *Phys. Lett.* A **32**, 221.
Spear, F. S., Hazen, R. M. & Rumble, E. 1981 *Am. Miner.* **66**, 100.
Tennakoon, D. T. B., Jones, W., Rayment, T., Schlögl, R., Klinowski, J. & Thomas, J. M. 1983*b* *Clay Miner.* (In the press.)
Tennakoon, D. T. B., Jones, W., Thomas, J. M., Ballantine, J. A. & Purnell, J. H. 1984 (In preparation.)
Tennakoon, D. T. B., Jones, W., Thomas, J. M., Williamson, L. J., Ballantine, J. A. & Purnell, J. H. 1983*a* *Proc. Indian Acad. chem. Sci.* **92**, 27.
Terasaki, O., Thomas, J. M. & Ramdas, S. 1984 *J. chem. Soc. chem. Commun.* 216.
Thomas, J. M. 1983*a* In *Inorganic chemistry: towards the 21st century* (ed. M. H. Chisholm), p. 445. A.C.S. Symposium Series no. 211.
Thomas, J. M. 1977 *Chem. Brit.* **13**, 175.
Thomas, J. M. 1979 *Nature, Lond.* **2**, **79**, 755.
Thomas, J. M. 1980 *New Scient.* 580.
Thomas, J. M. 1982*a* *Ultramicroscopy* **8**, 13.
Thomas, J. M. 1982*b* In *Intercalation chemistry* (ed. A. J. Jacobson & M. S. Whittingham), p. 56. New York: Academic Press.
Thomas, J. M., Adams, J. M., Tennakoon, D. T. B. & Graham, S. H. 1976 *A.C.S. Symposium* **163**, 298.
Thomas, J. M., Gonzalez-Calbet, J. J., Fyfe, C. A., Gobbi, G. C. & Nicol, M. 1983*c* *Geophys. Res. Lett.* **10**, 91.
Thomas, J. M., Jefferson, D. A., Mallinson, L. G., Smith, D. J. & Crawford, E. S. 1978–9*e* *Chemica Scripta* **14**, 167.
Thomas, J. M., Jefferson, D. A. & Millward, G. R. 1982*d* *J. Microscop. Spectroscop. Electron.* **7**, 315.
Thomas, J. M., Klinowski, J., Wright, P. A. & Roy, P. A. 1983*b* *Angewandte Chemie* **22**, 614.
Thomas, J. M. & Millward, G. R. 1982*e* *J. chem. Soc. chem. Commun.* **22**, 1380.
Thomas, J. M., Millward, G. R., Ramdas, S. & Audier, M. 1983*d* *A.C.S. Symposium Series* 218 (ed. G. D. Stucky & F. G. Dwyer), p. 181.
Thomas, J. M., Ramdas, S., Klinowski, J., Fyfe, C. A. & Gobbi, G. 1982*c* *J. phys. Chem.* **86**, 1247.
Tomeoka, K. & Buseck, P. R. 1983 *Nature, Lond.* **306**, 354.
Vaughan, D. E. W. 1984 *J. molec. Catal.* (In the press.)
Vaughan, D. E. W. & Lussier, R. 1980 *5th Zeolite International Conference, Naples* (ed. L. V. Rees), p. 94. London: Heydon.
Veblen, D. R. 1983*a* *Am. Miner.* **68**, 594.
Veblen, D. R. 1983*b* *Am. Miner.* **68**, 566.
Veblen, D. R. & Buseck, P. R. 1979 *Science, Wash.* **206**, 1398.




PHILOSOPHICAL TRANSACTIONS OF THE ROYAL SOCIETY A MATHEMATICAL, PHYSICAL & ENGINEERING SCIENCES

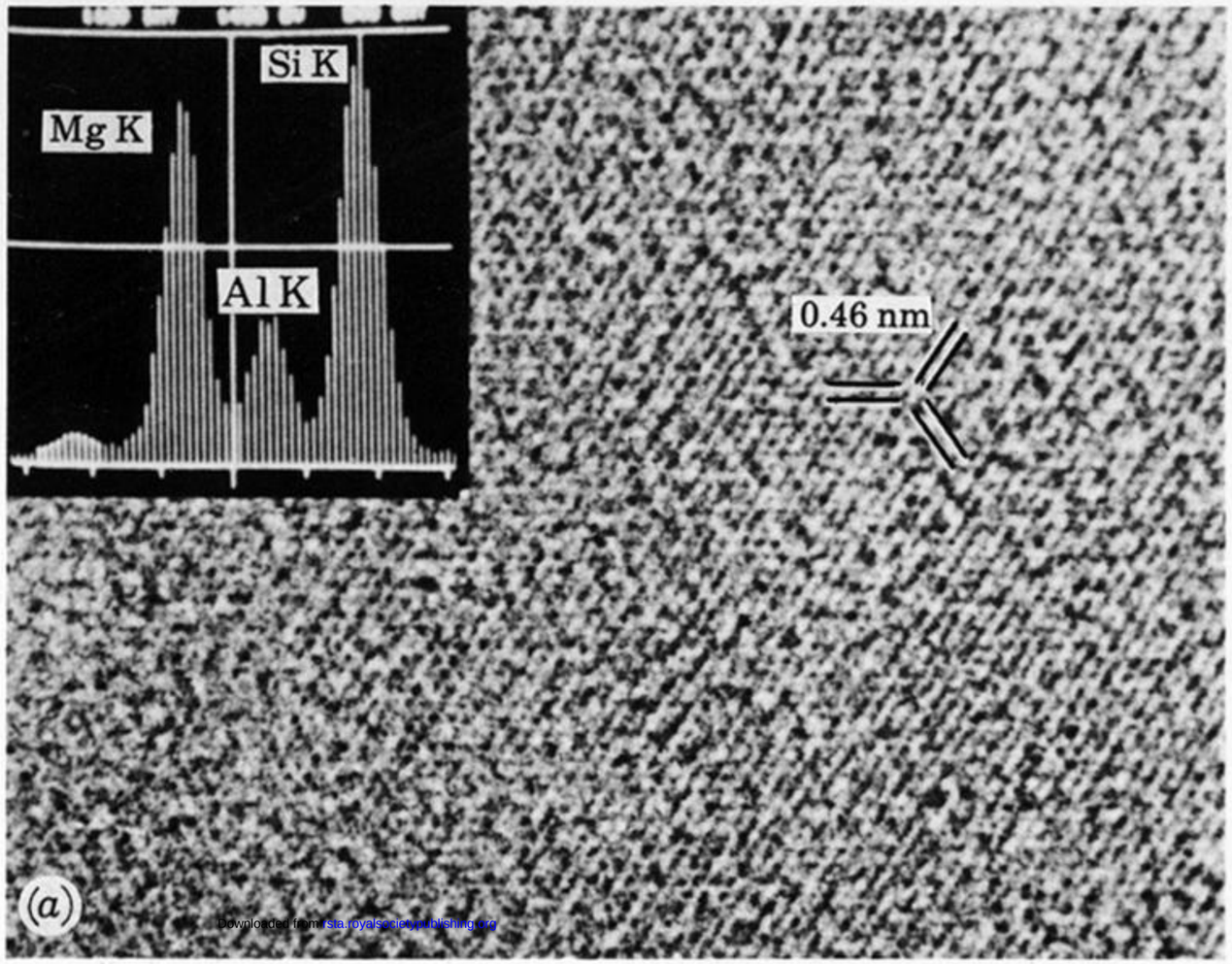


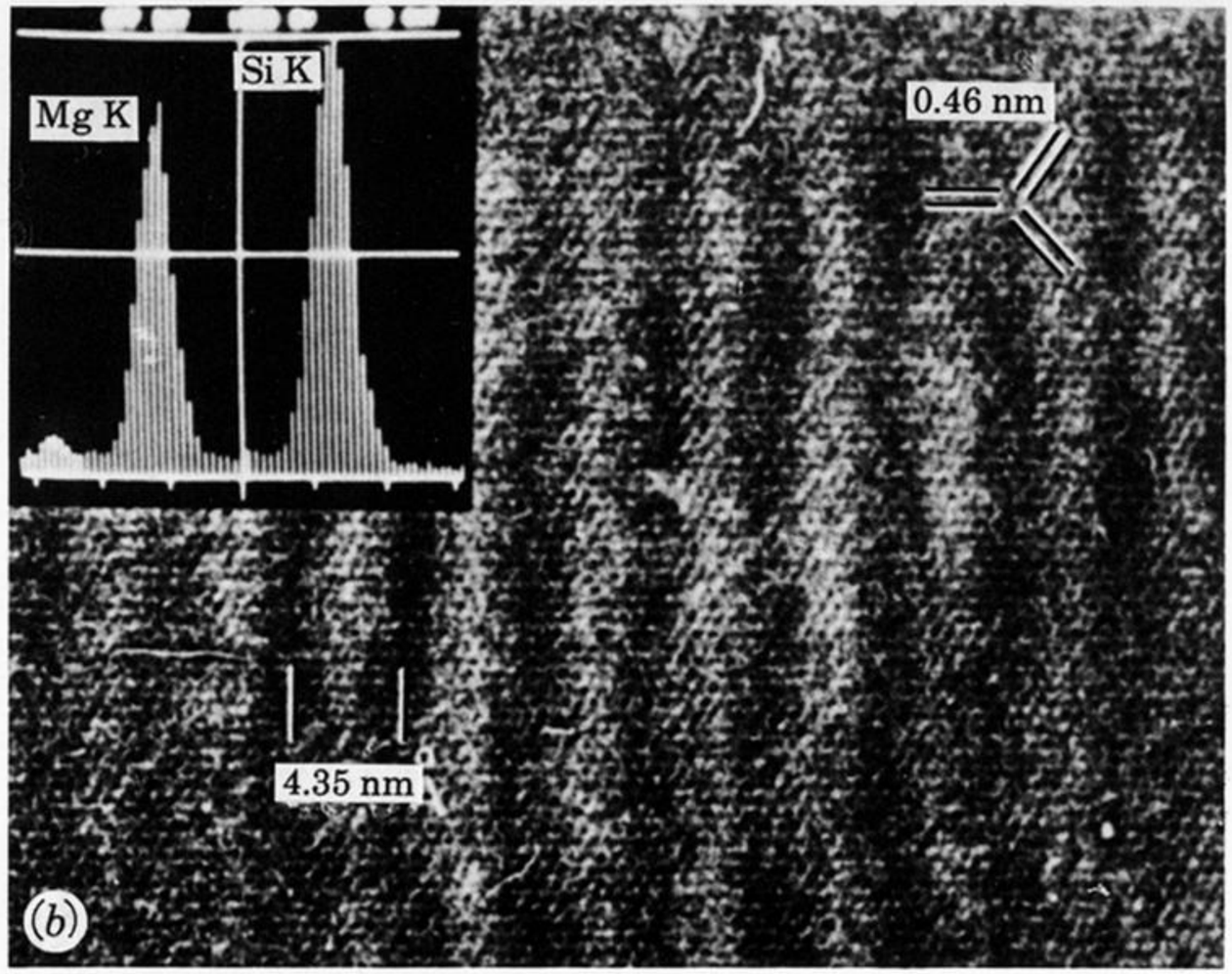


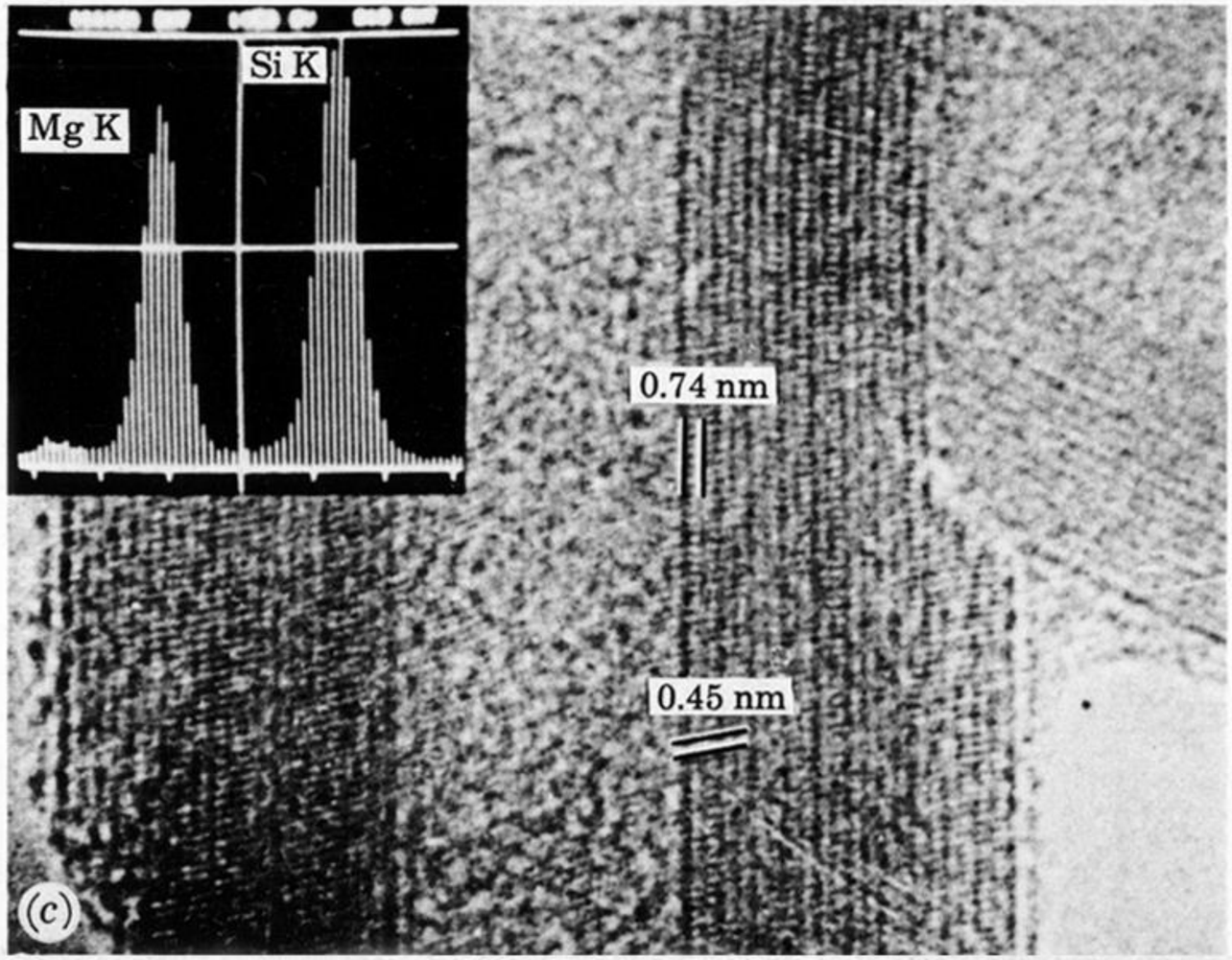


FIGURE 10. High-resolution electron microscopy micrographs and X-ray emission spectra of serpentines: (*a*) lizardite, (*b*) antigonite, showing the corrugation periodicity of *ca.* 4.3 nm, and (*c*) chrysotile, showing the interlayer spacing (0.74 nm).





PHILOSOPHICAL TRANSACTIONS OF THE ROYAL SOCIETY A MATHEMATICAL, PHYSICAL & ENGINEERING SCIENCES

PHILOSOPHICAL TRANSACTIONS OF THE ROYAL SOCIETY A MATHEMATICAL, PHYSICAL & ENGINEERING SCIENCES

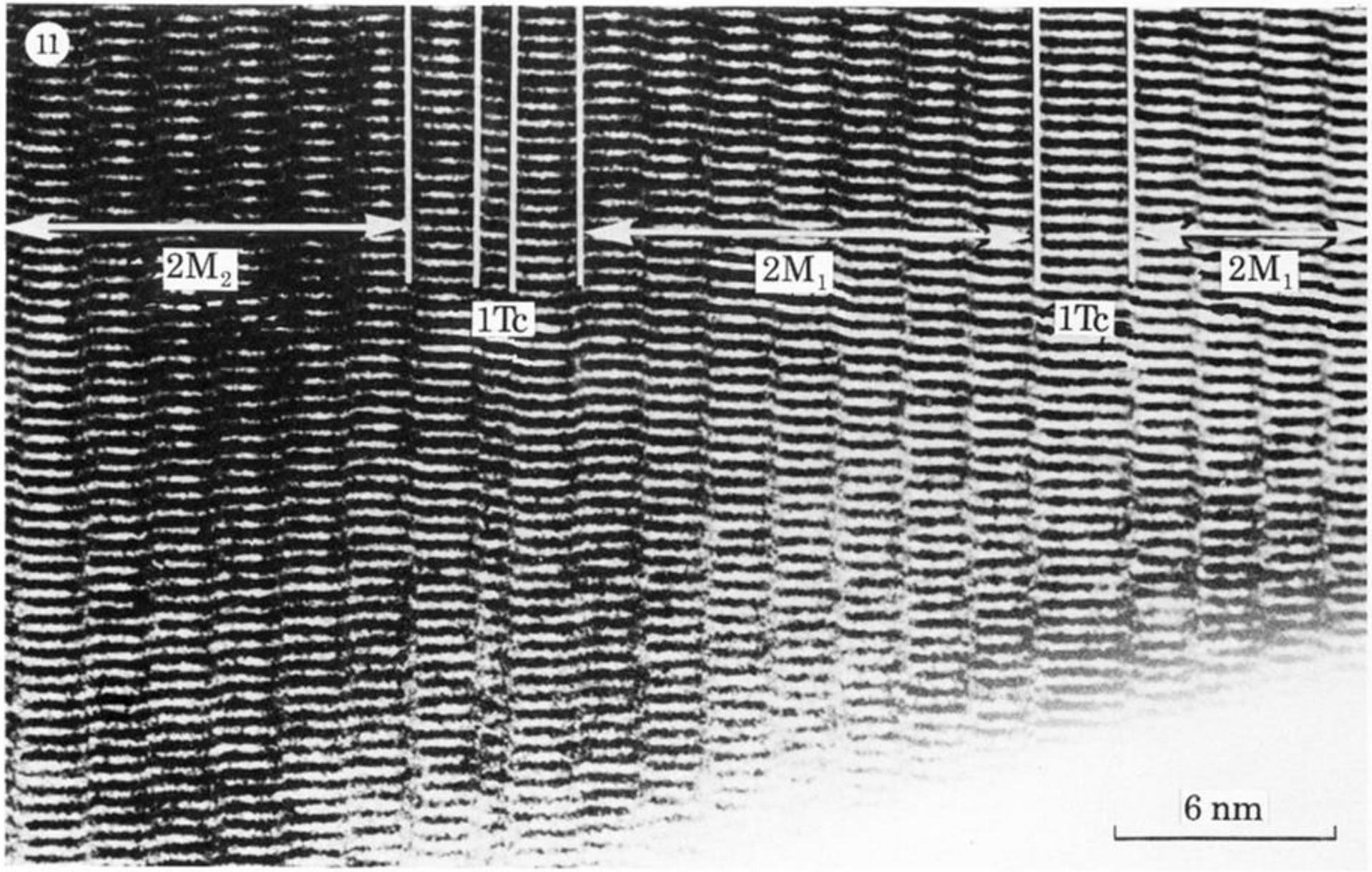


FIGURE 11. High-resolution electron microscopic image of a thin section of chloritoid showing intergrowths of various polytypes (see text).

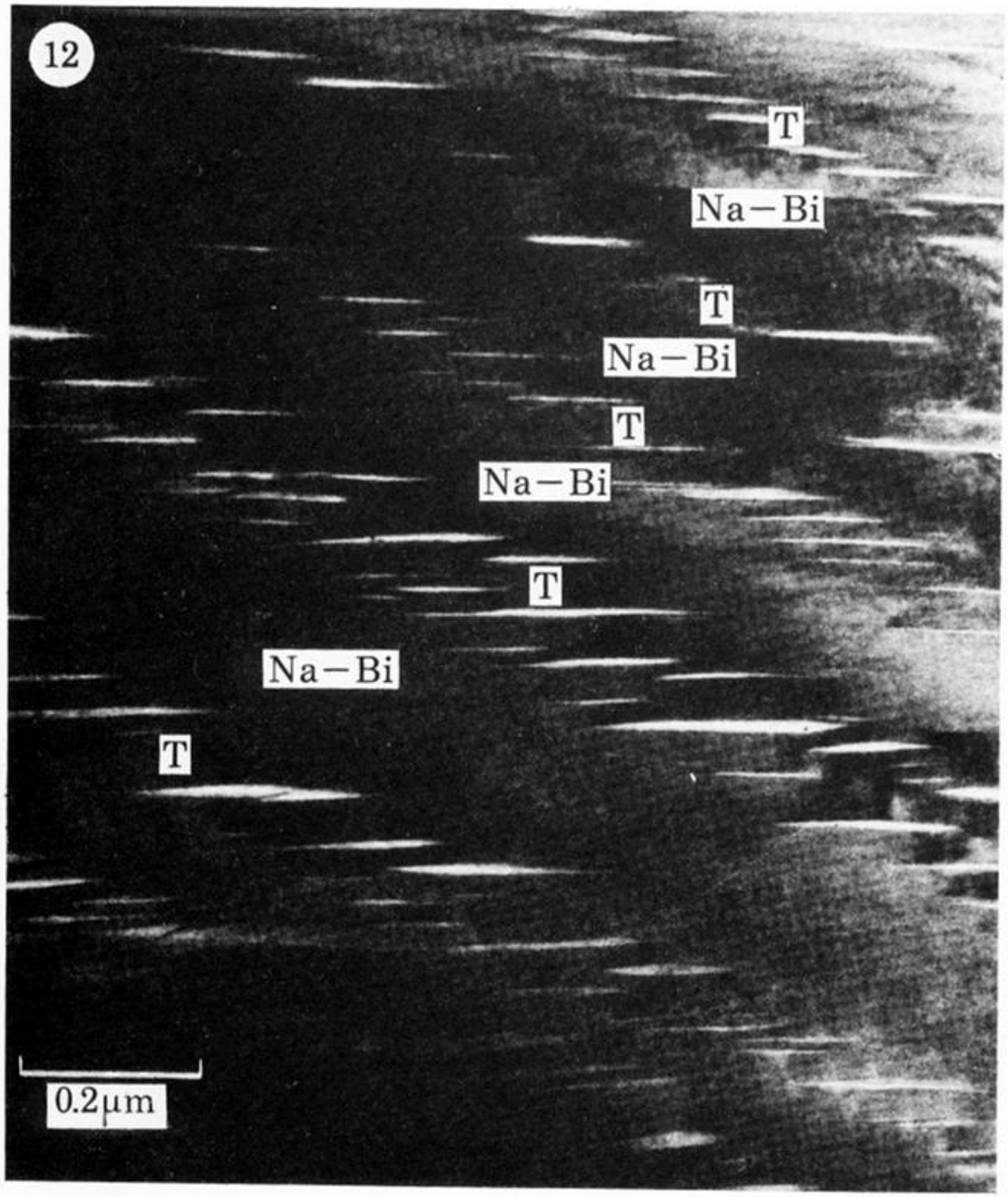


FIGURE 12*a*. Low-resolution bright-field electron micrograph of the lamellar microstructure in wonesite. Talc (T) and sodium biotite (Na–Bi) lamellae are titled with respect to the plane (001), which is horizontal. The talc lamellae can be recognized by the white, lenticular voids parallel to (001). (*b*) Schematic drawing of this microstructure, emphasizing that the lamellae are not parallel to the structural layers. Circles represent interlayer alkali sites. (After Veblen 1983*a*.)

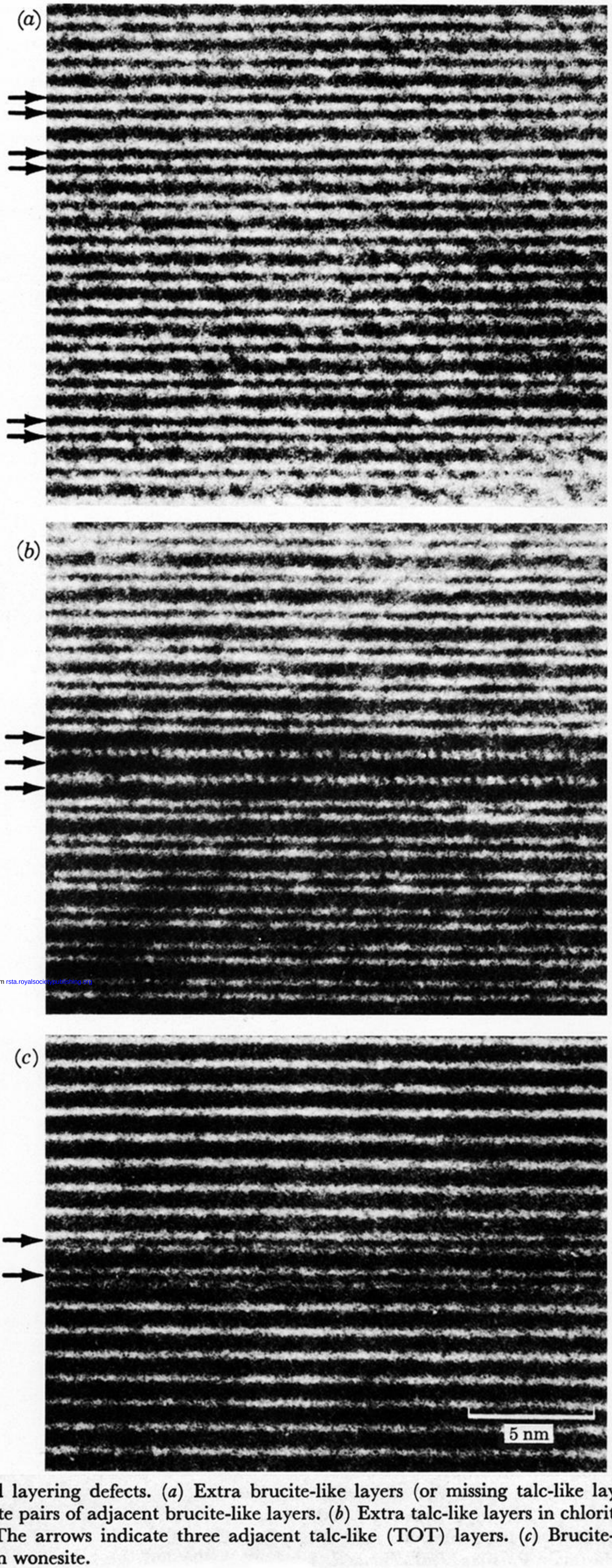




GURE 13. Mixed layering defects. (*a*) Extra brucite-like layers (or missing talc-like layers) in chlorite. The arrows indicate pairs of adjacent brucite-like layers. (*b*) Extra talc-like layers in chlorite (or missing brucite-like layers). The arrows indicate three adjacent talc-like (TOT) layers. (*c*) Brucite-like layers (arrowed) intercalated in wonesite.